Near-Infrared Resonant Nanoshells for Combined Optical Imaging and Photothermal Cancer Therapy

André M. Gobin,[†] Min Ho Lee,[†] Naomi J. Halas,[‡] William D. James,[§] Rebekah A. Drezek,[†] and Jennifer L. West*,[†]

Department of Bioengineering, Rice University, Houston, Texas 77005, Department of Electrical and Computer Engineering, Rice University, Houston, Texas 77005, and Center for Chemical Characterization and Analysis, Texas A&M University, College Station, Texas 77843

ABSTRACT

Metal nanoshells are core/shell nanoparticles that can be designed to either strongly absorb or scatter within the near-infrared (NIR) wavelength region (∼650−950 nm). Nanoshells were designed that possess both absorption and scattering properties in the NIR to provide optical contrast for improved diagnostic imaging and, at higher light intensity, rapid heating for photothermal therapy. Using these in a mouse model, we have demonstrated dramatic contrast enhancement for optical coherence tomography (OCT) and effective photothermal ablation of tumors.

Much of the promise for nanotechnology in medicine has focused on the development of multifunctional agents for integrated diagnosis and therapy.[1,2] Here we report on a successful in vivo demonstration of the use of near-infrared resonant nanoparticles, gold nanoshells, to first increase optical contrast in tumors for optical coherence tomography (OCT) imaging and second, to subsequently treat the tumors using nanoshell absorption of near-infrared (NIR) light for photothermal ablation using a single-nanoparticle formulation that has been designed to have both absorption and scattering in the NIR.

Nanoshells consist of a dielectric core nanoparticle surrounded by an ultrathin metal shell with tunable plasmon resonances. Nanoshells offer the ability to manipulate both the resonant wavelength and the relative scattering and absorption efficiencies through the size and composition of each layer of the nanoshell structure.[3−5] Given these advantages, nanoshells can be used as contrast agents for enhanced OCT imaging,[6,7] based on their backscattering properties, as well as cancer therapeutics,[8,9] due to their absorbing properties. Through appropriate nanoparticle design for both strong absorption and scattering, both imaging and therapy should be improved with a single-particle formulation. For these studies, nanoshells were designed for absorption and scat-

tering in the near-infrared (NIR) region.[4,10] This region is of significant biological importance, as it provides a region in the spectrum useful for both therapeutic and imaging applications in tissue because the components of tissue do not have significant absorption in this range of wavelengths.[11] Nanoshells are currently being investigated for use in the NIR region for a variety of applications, including diagnostic assays,[12] modulated drug delivery systems,[13] and for laser tissue welding.[14] We have previously demonstrated photothermal ablation and complete regression of tumors in mice, accomplished through intravenous injection and subsequent passive tumor accumulation, which was followed by external NIR treatment for several minutes.[8,9] We recently reported the development of gold nanoshells suitable for therapy and imaging of cancer cells in in vitro studies.[6,15] This early work imaged human breast cancer cells that had been treated with antibody-conjugated gold nanoshells under darkfield microscopy, followed by NIR laser, inducing cell ablation only within the laser spot. In the present study, we report on the use of nanoshells as contrast agents to enhance OCT imaging of tumors grown in vivo followed by therapeutic application of NIR light.

OCT is an imaging modality that provides cross-sectional subsurface imaging of biological tissue with micrometer-scale resolution. The principles of OCT have been described previously.[16,17] OCT uses a short coherence length light source in a Michelson interferometer to enable high-resolution optical sectioning in tissue. In the system used in this study, low coherence light emitted from the source is

* Corresponding author. E-mail: jwest@rice.edu. Telephone: (713) 348-5955. Fax: (713) 348-5877. Rice University, MS 142, Department of Bioengineering, 6100 S. Main St., Houston, TX 77251.
† Department of Bioengineering, Rice University.
‡ Department of Electrical and Computer Engineering, Rice University.
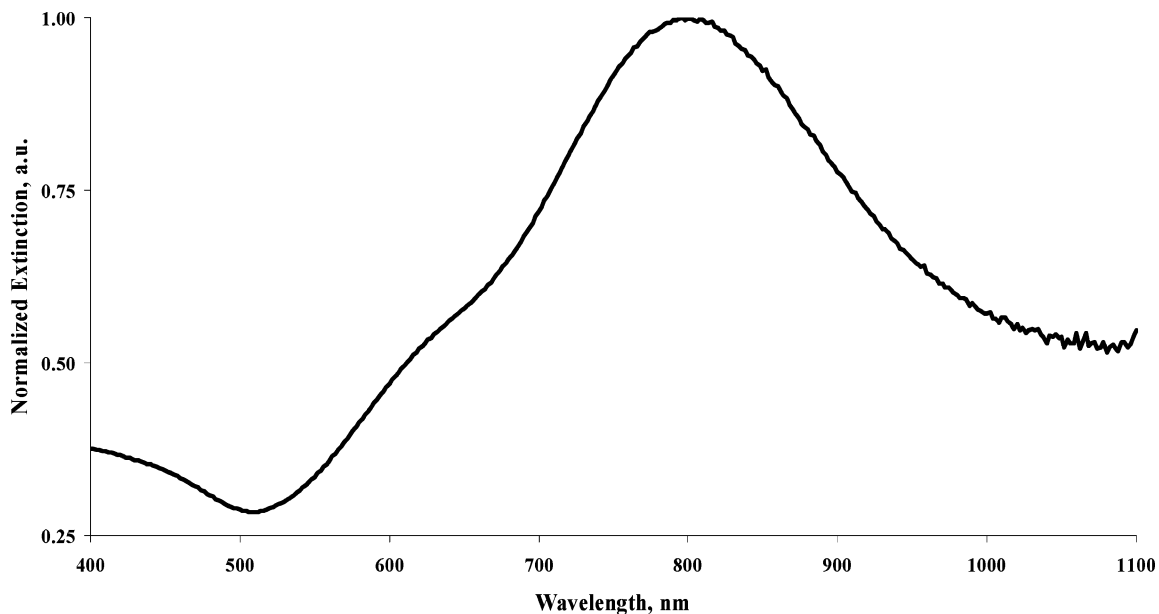§ Center for Chemical Characterization and Analysis, Texas A&M University.

Figure 1. Extinction spectra of nanoshells used in this study. Nanoshells are 143 nm in diameter with a core of 119 nm and a shell thickness of 12 nm.

directed onto a beam splitter. One beam is sent toward a reference mirror of known path length distance while the other is directed toward the sample. The reflected waves from both the reference mirror and sample are recombined at the beam splitter and directed to a detector where interference patterns are monitored as the reference mirror is moved. By monitoring these patterns while scanning the reference mirror, it is possible to map depth-resolved reflectivity of the tissue. The diagnostic potential of OCT was demonstrated by Matheny et al.[18] and has been used for imaging cancers of the gastrointestinal system,[19−22] prostate,[23] and oral mucosal[24] among others.

The use of contrast agents in OCT offers the promise of enhanced diagnostic power, similar to results with contrast agents in computed tomography (CT) and magnetic resonance imaging (MRI). To increase contrast in OCT, imaging agents including microbubbles[25] and microspheres with gold nanoparticles have been employed.[26,27] Optimal contrast agents for OCT would both further enhance contrast in vivo over the ∼5% improvement obtained with microbubbles and offer a smaller alternative to engineered microspheres (∼2−15 μm) to improve distribution into the microcirculation. Because of their biocompatibility, tunable optical properties, and small scale size, nanoshells are well suited to OCT, providing easily detected backscattering of NIR light. Furthermore, nanoshells have been shown to accumulate in tumors due to the leakiness of tumor vasculature, allowing efficient delivery of quantities suitable for both imaging and therapy. For this reason, the current work combines the use of OCT imaging with NIR treatment using an NIR absorbing and scattering nanoshell in a murine in vivo model.

Design of Dual Function Nanoshells. Nanoshells were made with cores that were 119 ± 11 nm in diameter. The shell thickness was approximately 12 nm. The measured extinction spectra of the nanoshells used in this study are shown in Figure 1. Mie theory scattering calculations predict

that these particles have approximately 67% of the extinction due to absorption and 33% due to scattering at 800 nm.

Nanoshells were prepared as previously described.[4,5] Briefly, silica cores were grown using the Stöber process, the basic reduction of tetraethyl orthosilicate (Sigma-Aldrich, Milwaukee, WI) in ethanol. The resultant silica nanoparticles were examined under scanning electron microscopy (SEM; Philips FEI XL30), and particles with a polydispersity of less than 10% were used in subsequent steps. Reaction of the silica core nanoparticles with (3-aminopropyl) triethoxysilane (APTES, Sigma-Aldrich) provided amine groups on the surface of the core to allow for adsorption of gold colloid. Gold colloid was prepared to a size of 2−4 nm in the method of Duff et al. and aged 2−3 weeks at 4 °C.[28] The colloid was then concentrated 20× through rotary evaporation and mixed with the aminated silica particles, allowing small gold colloid, attached to the larger silica nanoparticle surface, to act as nucleation sites in the subsequent reduction step. This final step, growing the gold shell, was accomplished by the reduction of gold from chloroauric acid ($HAuCl_4$) in the presence of formaldehyde. By this method, the reduction of gold around the initial colloid sites allows gold islands to develop and eventually coalesce to form a contiguous gold shell. The extinction characteristics of the nanoshells were determined using a UV−vis spectrophotometer (Carey 50 Varian, Walnut Creek, CA). Nanoshells were surface-coated with poly(ethylene glycol) PEG to enhance circulation times and reduce immune response. Pegylation was accomplished by adding 20 μL of 5 μM PEG-SH, molecular weight 5 kDa (Nektar, Huntsville, AL) to 1.5×10^{10} nanoshells/mL in DI water for a minimum of 8 h. PEG-modified nanoshells were sterilized by filtration using a 0.22 μm filter and subsequently concentrated by centrifugation and re-diluted with sterile phosphate buffered saline (PBS).

Nanoshells Provide Significant Increase in OCT Contrast. PEG-modified nanoshells were injected intravenously
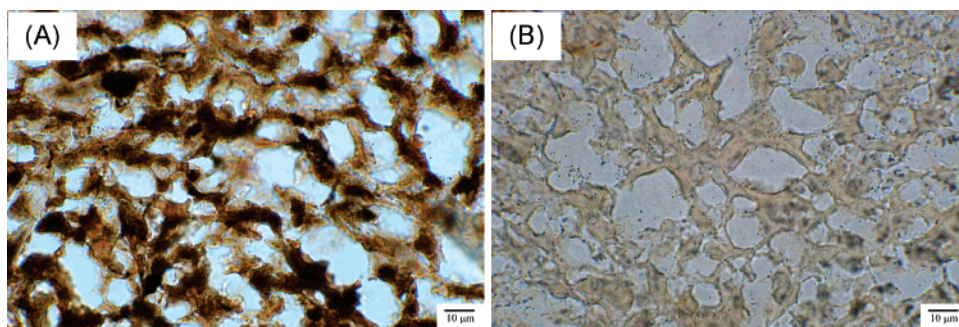
Figure 2. Silver enhancement staining of tissue shows heterogeneous staining of the tumor tissue from mice injected with nanoshells (A) indicating the presence of nanoshells. In contrast, there is little silver enhancement of sections taken from mice with PBS injection (B).

in tumor-bearing mice and allowed to passively accumulate in the tumor tissue due to the leakiness of the tumor vasculature. The significant accumulation of particles within the tumor tissue dramatically increased the NIR scattering within the tumor, enhancing the OCT contrast.

To grow tumors in mice, colon carcinoma cells were cultured and then injected subcutaneously in mice. Murine colon carcinoma cells (CT-26, ATCC, Manassas, VA) were grown at 37 °C in a 5% CO_2 environment in RPMI media supplemented with 4 mM l-glutamine, 1% penicillin, 1% streptomycin, and 10% fetal bovine serum (FBS). Cells were detached from culture with trypsin (0.05%) and EDTA (0.02%). Cells were re-suspended in sterile PBS for inoculation into BALBc mice (Charles River, Willington, MA). BALBc mice were used under an approved protocol of the Institutional Animal Care and Use Committee at Rice University. 150 000 CT-26 cells suspended in 25 μL of PBS were inoculated subcutaneously in the right flank of mice. Tumors were allowed to grow to a diameter of approximately 5 mm (~10 days). At that point, 150 μL of PEG-modified nanoshells in PBS (1.5×10^{11} nanoshells/mL) were injected into the tail vein 20 h prior to imaging via OCT. Control animals received a PBS injection.

In one set of mice, tumors were excised at 20 h, and nanoshell levels in tumor and normal tissues were assessed. Two methods were used for this. First, excised tumors were cryosectioned and silver stained (Sigma Silver Enhancement system, Sigma, Milwaukee, WI); silver staining allows the nanoshells to act as nucleation sites for deposition of silver to grow large enough to allow for visualization under light microscopy. Other tissue samples were lyophilized for gold content determination using neutron activation analysis (NAA).[29] The blank and the tumor sample were irradiated along with precise calibration standards at the Texas A&M University's Nuclear Science Center 1 MW TRIGA research reactor for 14 h. The irradiation position used in this study has an average neutron flux of approximately 1×10^{13} s^{-1} cm^{-2}. High-purity germanium detectors with nominal resolutions (fwhm) of 1.74 keV or better and efficiencies of 25−47% by industry standard relative measurement were used to quantify the 412 keV gamma line from ^{198}Au. The Canberra Industries OpenVMS alpha processor-based Genie-ESP software was used for acquisition and computation of gold concentrations.

Histological examination of tumors using silver staining confirmed the presence of nanoshells throughout the tumors. Figure 2 shows the silver staining of representative areas of tumors from mice treated with nanoshells (A) or with PBS (B). Additionally, NAA verified nanoshells present in the tumor shown in Figure 2A at 12.5 ppm, which is equivalent to approximately 3 million nanoshells per gram of tumor tissue, compared to 0 ppm for tumors of mice injected with just PBS 2B.

OCT images were collected for nanoshell-injected and control mice 20 h following injection (to allow time for passive accumulation of nanoshells) and analyzed to assess the increase in contrast provided by the nanoshells in tumor tissue compared to normal tissue. This study used a commercially available OCT imaging system (Niris Imaging System, Imalux, Cleveland, OH). The axial and transverse resolutions were measured to be approximately 10 and 15 μm, respectively. OCT images of the tumor and normal tissue was taken after 20 h of circulation. The animals were not anesthetized during the injection or circulation period, only during imaging and treatment. The tumors were imaged using the Niris OCT imaging device by applying glycerol on the shaved tumor site for index matching and placing the probe in contact with the skin directly above the tumor. Images were captured at several locations on each tumor through the integrated computer and image analysis system. Normal tissue images were taken at a location at least 2 cm distant to the tumor on the same animal. Images were analyzed to first quantify the contrast levels using standard thresholding for image analysis, then intensity data were analyzed using an unpaired Student t test assuming equal variance with a confidence interval of 95%, $\alpha < 0.05$ of the two populations of images from PBS-treated and nanoshell-treated mice. Analysis of the tumor regression was performed using the average measurements of the tumor size of the surviving populations at the times shown and compared using an unpaired Student t test assuming equal variance with a confidence interval of 95%, $\alpha < 0.05$.

Figure 3 shows OCT imaging results obtained after PBS injection, panels A and C, and after nanoshell injections, panels B and D. The strata of the skin and underlying muscle can be seen in the OCT image of the normal tissue panel A and B. There is no enhancement in layers of normal tissue in mice treated with nanoshells compared with the PBS-
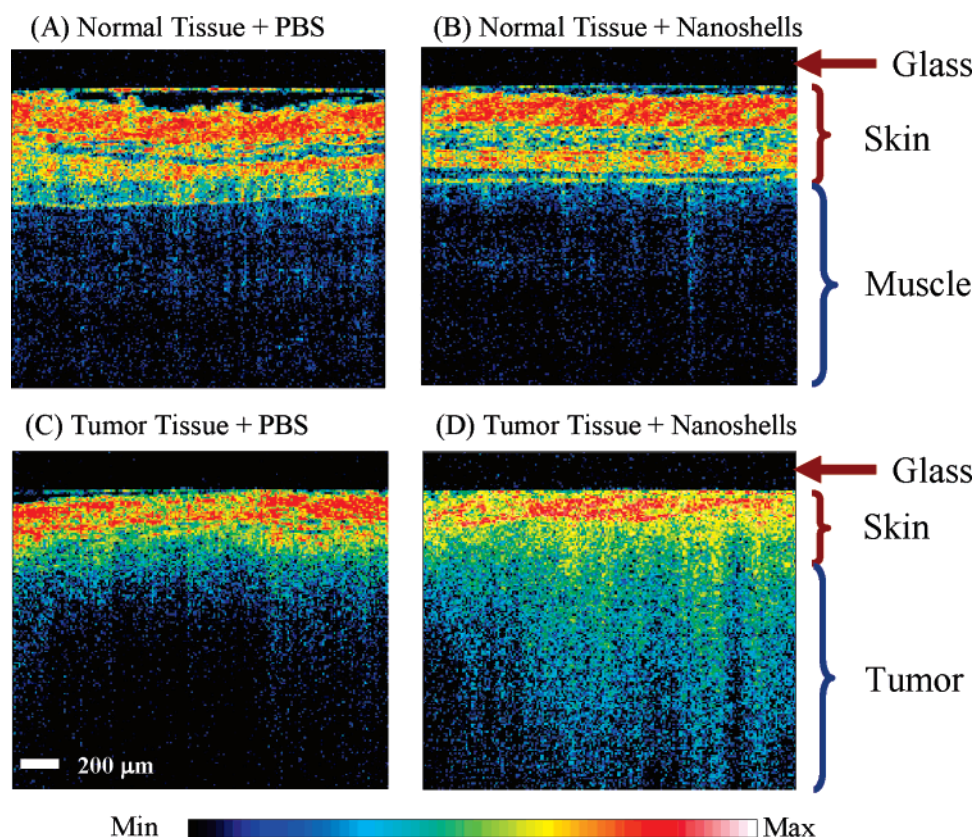
(A) Normal Tissue + PBS   (B) Normal Tissue + Nanoshells

Glass
Skin
Muscle

(C) Tumor Tissue + PBS   (D) Tumor Tissue + Nanoshells

Glass
Skin
Tumor

200 μm

Min   Max

Figure 3. Representative OCT images from normal skin and muscle tissue areas of mice systemically injected with nanoshells (A) or with PBS (B). Representative OCT images from tumors of mice systemically injected with nanoshells (C) or with PBS (D). Analysis of all images shows a significant increase in contrast intensity after nanoshell injection in the tumors of mice treated with nanoshells while no increase in intensity is observed in the normal tissue. The glass of the probe is 200 μm thick and shows as a dark nonscattering layer.
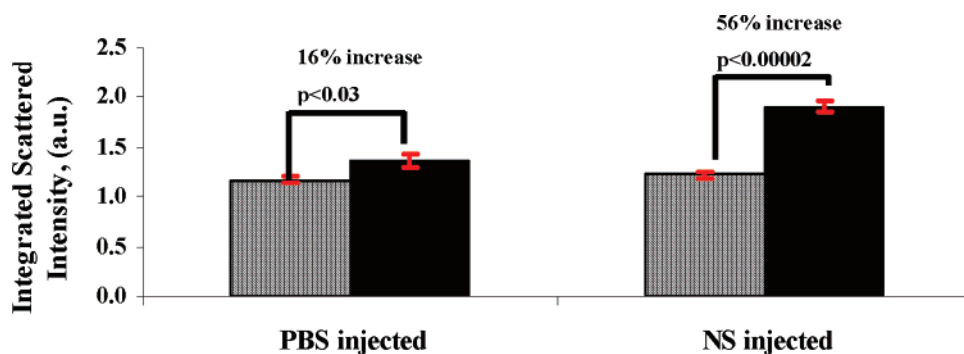

Figure 4. Quantification of OCT images shows a significant increase in intensity of images of tumors from mice with systemic nanoshell injection. Normal muscle tissue is shown in the blue bar while tumor tissue is shown in the black bar. Values are average ± SEM; p values are shown.

injected mouse because nanoshells do not extravasate appreciably into normal tissues.

The enhanced brightness of the image in panel D relative to panel C of Figure 3, where nanoshells have accumulated in the tumor, indicates that gold nanoshells can provide substantial contrast in OCT imaging. Figure 3D also shows that the borders of tumors (on the left) can more easily be discerned in the OCT images of nanoshell-treated mice compared to those mice that had only PBS injection (Figure 3C). Figure 4 shows the quantification of the image intensity of OCT images of normal tissue ($n = 3$) and tumor tissue ($n = 6$) with PBS injections and nanoshell injections. Images were analyzed to first quantify the contrast and then analyzed

using a Student's t test of the two populations of images from PBS-treated and nanoshell-treated mice. The data show a significant increase in the optical contrast of tumor compared to normal tissue when nanoshells are used, $p < 0.00002$. No statistical difference is observed in the intensity of the optical contrast of images of normal tissue whether nanoshells are used or PBS.

Nanoshells Also Allow Photothermal Ablation of Tumors with Increased Survival. As described above, tumor-bearing mice received either nanoshell or PBS injections. Animals were randomly assigned to control and treatment groups. Animals were randomly divided into three groups: treatment (nanoshell + laser); sham (PBS + laser), and
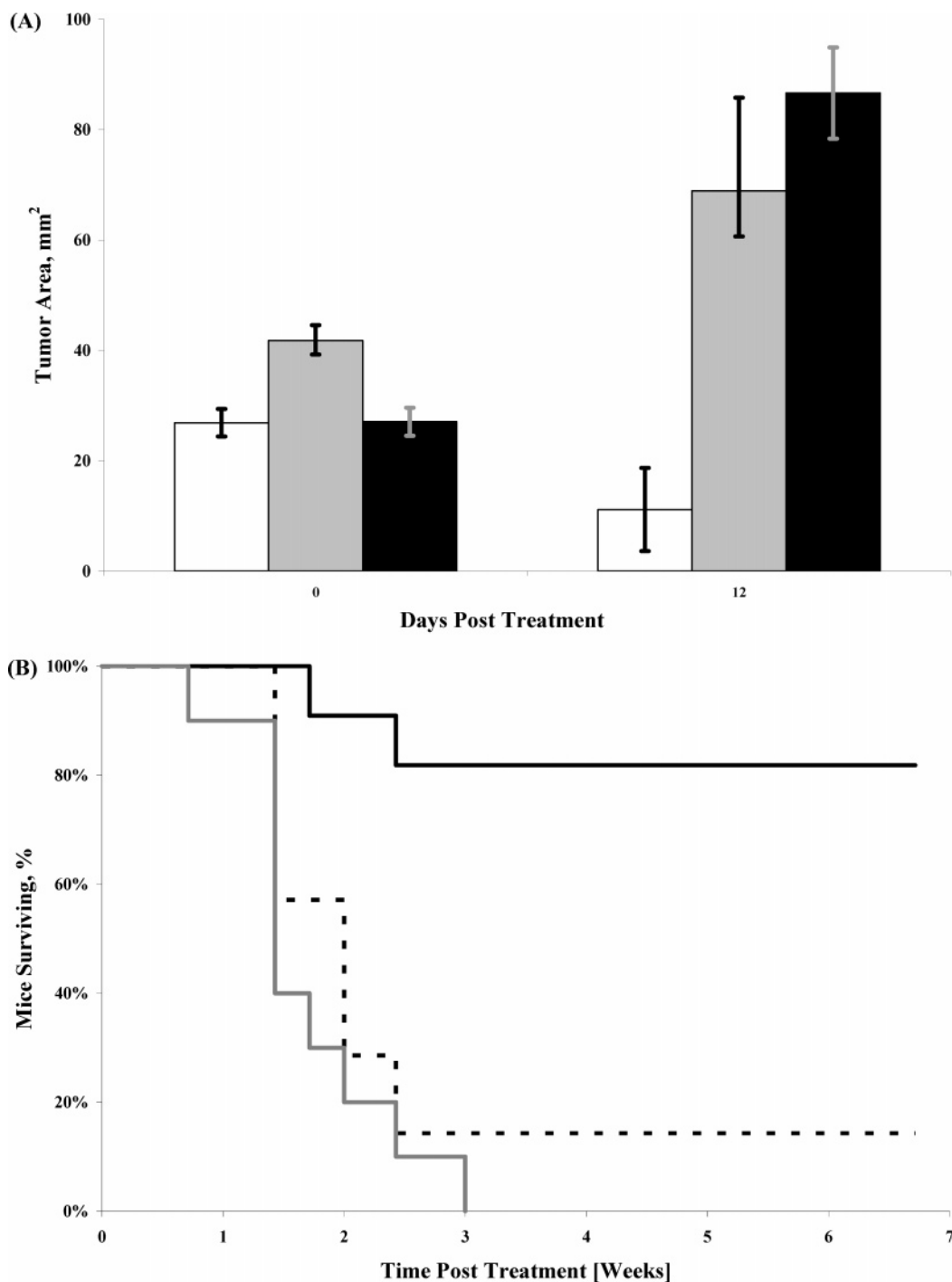
Figure 5. (A) Tumor size before irradiation and 12 days post-irradiation of mice treated with nanoshell + NIR laser irradiation (white bar); PBS sham + NIR laser treatment (gray bar) or untreated control (black bar); values are average ± SEM. (B) Kaplan−Meier survival data for the treatment groups post irradiation; nanoshell + NIR laser irradiation (solid black line); PBS sham + NIR laser treatment (dashed black line) or untreated control (gray line); survival was followed for 7 weeks posttreatment. After 21 days, the nanoshell therapy group survival rate was significantly higher than either control group, $p < 0.001$.

control (untreated). Following OCT imaging as described above, animals in the treatment and sham groups had their tumors irradiated with a NIR laser. In vivo irradiation was accomplished using an Integrated Fiber Array Packet, FAP-I System, with a wavelength of 808 nm (Coherent, Santa Clara, CA) at a power density of 4 W/cm^2 and a spot size of 5 mm diameter for 3 min. Tumor size and animal survival was monitored for 7 weeks after imaging and treatment. Survival

data analysis was performed using the standard Kaplan−Meier analysis using MedCalc software.

Figure 5A shows the tumor sizes on the day of treatment and 12 days after treatment; tumors on all but two nanoshell-treated mice had completely regressed. Figure 5B shows the survival of the mice during the entire study period. Kaplan−Meier statistical analysis shows a median survival of 14 days for the PBS + laser group and 10 days for the untreated

control group. By day 21, the survival of the nanoshell + laser group was significantly greater than either the control or sham groups, $p < 0.001$, and this then continued for the duration of the study. Median survival time could not be calculated for this group, as the long-term survival was 83%.

We have reported the successful in vivo demonstration of a single nanoparticle that enhances the scattering signal for OCT imaging while retaining its properties to affect photo-thermal ablation of the tumor. Our findings suggest that engineered nanoparticles, such as nanoshells with tunable optical properties, can indeed play a vital role in a number of emerging in vivo molecular imaging modalities and allow integration of diagnostic and therapeutic technologies.

References

(1) Sullivan, D. C.; Ferrari, M. *Mol. Imaging* **2004**, *3*, 364−369.
(2) Ferrari, M. *Nat. Rev. Cancer* **2005**, *5*, 161−171.
(3) Averitt, R.; Wescott, S.; Halas, N. *J. Opt. Soc. Am. B* **1999**, *6*, 1824−1832.
(4) Oldenburg, S. J.; Averitt, R. D.; Westcott, S. L.; Halas, N. J. *Ch. Phys. Lett.* **1998**, *288*, 243−247.
(5) Oldenburg, S. J.; Jackson, J. B.; Westcott, S. L.; Halas, N. J. *Appl. Phys. Lett.* **1999**, *75*, 2897−2899.
(6) Loo, C.; Lowery, A.; Halas, N.; West, J.; Drezek, R. *Nano Lett.* **2005**, *5*, 709−711.
(7) Loo, C. H.; Lin, A.; Hirsch, L.; Lee, M.; Barton, J. K.; Halas, N. J.; West, J. L. *Technol. Cancer Res. Treat.* **2004**, *3*, 33−40.
(8) Hirsch, L. R.; Stafford, R. J.; Bankson, J. A.; Sershen, S. R.; Rivera, B.; Price, R. E.; Hazle, J. D.; Halas, N. J.; West, J. L. *Proc. Natl. Acad. Sci. U.S.A.* **2003**, *100*, 13549−13554.
(9) O'Neal, D. P.; Hirsch, L. R.; Halas, N. J.; Payne, J. D.; West, J. L. *Cancer Lett.* **2004**, *209*, 171−176.
(10) Averitt, R. D.; Westcott, S. L.; Halas, N. J. *J. Opt. Soc. Am. B* **1999**, *16*, 1824−1832.
(11) Weissleder, R. *Nat. Biotechnol.* **2001**, *19*, 316−317.
(12) Hirsch, L. R.; Jackson, J. B.; Lee, A.; Halas, N. J.; West, J. L. *Anal. Chem.* **2003**, *75*, 2377−2381.
(13) Sershen, S. R.; Westcott, S. L.; Halas, N. J.; West, J. L. *J. Biomed. Mater. Res. A* **2000**, *51*, 293−298.
(14) Gobin, A.; O'Neal, D.; Watkins, D.; Halas, N.; Drezek, R.; West, J. *Lasers Surg. Med.* **2005**, *37*, 123−129.
(15) Loo, C.; Hirsch, L.; Lee, M.-H.; Chang, E.; West, J.; Halas, N.; Drezek, R. *Opt. Lett.* **2005**, *30*, 1012−1014.
(16) Fujimoto, J. G.; Brezinsky, M. E.; Tearney, G. J.; Boppart, S. A.; Bouma, B.; Hee, M. R.; Southern, J. F.; Swanson, E. A. *Nat. Med.* **1995**, *1*, 970−972.
(17) Huang, D.; Swanson, E. A.; Lin, C. P.; Schuman, J. S.; Stinson, W. G.; Chang, W.; Hee, M. R.; Flotte, T.; Gregory, K.; Puliafito, C. A. *Science* **1991**, *254*, 1178−1181.
(18) Matheny, E. S.; Hanna, N. M.; Jung, W. G.; Chen, Z.; Wilder-Smith, P.; Mina-Araghi, R.; Brenner, M. *J. Biomed. Opt.* **2004**, *9*, 978−981.
(19) Li, X. D.; Boppart, S. A.; Dam, J. V.; Mashimo, H.; Mutinga, M.; Drexler, W.; Klein, M.; Pitris, C.; Krinsky, M. L.; Brezinski, M. E.; Fujimoto, J. G. *Endoscopy* **2000**, *32*, 921−930.
(20) Izatt, J. A.; Kulkarni, M. D.; Wang, H.-W.; Kobayashi, K.; Sivak, M. V. *IEEE J. Sel. Top. Quantum Electron.* **1996**, *4*, 1017−1028.
(21) Tearney, G. J.; Brezinski, M. E.; Southern, J. F.; Bouma, B. E.; Boppart, S. A.; Fujimoto, J. G. *Am. J. Gastroenterol.* **1997**, *92*, 1800−1804.
(22) Kobayashi, K.; Izaat, J.; Kulkarni, M.; Willis, J.; Sivak, M. *Gastrointest. Endosc.* **1998**, *47*, 515−523.
(23) D'Amico, A. V.; Weinstein, M.; Li, X.; Richie, J. P.; Fujimoto, J. G. *Urology* **2000**, *55*, 783−787.
(24) Sergeev, A. M.; Gelikonov, V. M.; Gelikonov, G. V.; Feldchtein, F. I.; Kuranov, R. V.; Gladkova, N. D. *Opt. Exp.* **1997**, *1*, 432−440.
(25) Barton, J. K.; Hoying, J. B.; Sullivan, C. J. *Acad. Radiol.* **2002**, *9*, S52−S55.
(26) Lee, T. M.; Oldenburg, A. L.; Sitafalwalla, S.; Marks, D. L.; Luo, W. *Opt. Lett.* **2003**, *28*, 1546−1548.
(27) Oldenburg, A. L.; Hansen, M. N.; Zweifel, D. A.; Wei, A.; Boppart, S. A. *Opt. Exp.* **2006**, *14*, 6724−6738.
(28) Duff, D. G.; Baiker, A.; Edwards, P. P. *Langmuir* **1993**, *9*, 2301−2309.
(29) James, W. D.; Hirsch, L. R.; West, J. L.; O'Neal, P. D.; Payne, J. D. *J. Radioanal. Nucl. Chem.* **2006**, *271*, 455−459.

NL070610Y